

Neural Network for Phase Diagrams of Polymer-containing Liquid Mixtures

Issei Nakamura^{*}

[†]*Department of Physics, Michigan Technological University, Houghton, Michigan 49931, United States*

^{*}*inakamur@mtu.edu*

We develop a deep neural network (DNN) that accounts for the phase behaviors of polymer-containing liquid mixtures. The key component in the DNN consists of a hidden layer that captures the characteristic features of phase behavior via coarse-grained mean-field theory and scaling laws and substantially enhances the accuracy of the DNN. Moreover, this hidden layer enables us to reduce the size of the DNNs for the phase diagrams. This study also presents the predictive power of the DNN for the phase behaviors of polymer solutions and salt-free and salt-doped diblock copolymer melts.

Phase separation of polymer-containing liquid mixtures is ubiquitous in a broad spectrum of science and engineering. It is necessary to analyze the abundant and diverse experimental data obtained concurrently; however, this process may be a daunting task when experimental settings and material properties are altered, and simulations may not assess the relevant time scale of phase separation. Furthermore, accurate correspondence among an experiment, theory, and simulation often becomes unclear. In this Letter, we present a third approach by developing a DNN for the phase behavior of liquid mixtures. In the current study, the DNN does not require many neurons and hidden layers and is thus computationally feasible on common workstations. Note that convolutional neural networks consist of convolutional and pooling layers for extracting the characteristic features of visual imagery and reducing the dimension of input data [1]. Inspired by this perspective, we construct the first hidden layer via coarse-grained mean-field theory and scaling laws, and this layer captures the representative features of target systems. This layer also allows us to ease local minimum problems in loss functions that evaluate the accuracy of NNs [1].

NNs have drawn considerable attention in solving real-world problems in a broad spectrum of research areas and have already shown their remarkable efficacy in solving practical scientific problems [2-12]. Early examples for molecular separation include the study by Dai, Sumpter and Noid, who developed an early type of NN that accounted for the phase boundary of the macroscopic phase separation of binary molten-salt mixtures [13]. Later, NNs were used to consider the phase diagrams for microemulsion-based drug delivery systems involving oil, water and surfactants [14]. The architecture of the NN was relatively simpler than those of the recent DNNs, yet the NN tuned with only 171 training data points became remarkably consistent with the experimental pseudo-ternary phase diagrams. Several studies related to microemulsions for drug delivery systems further provided the proof-of-concept that NNs may have excellent predictive power for the phase behavior of liquid mixtures [15-20]. Nevertheless, the development of NNs for the phase behavior of polymer-containing liquid mixtures remains significantly limited. Moreover, there are technical requirements that appear to substantially restrict

the use of NNs by non-experts in machine learning. For example, NNs are typically trained by a gradient-descent optimization algorithm such as a backpropagation algorithm using package code or computer software. However, the loss function typically involves many local minima, which substantially declines the efficiency of the backpropagation method because the gradient descent gets trapped in local minima. Moreover, the landscape of the loss function often has many saddle points, at which the gradient becomes zero. This feature also significantly slows down the update process of model parameters (weights) when the backpropagation algorithm is invoked. Additionally, the initial guess of the model parameters is also often critical in training NNs.

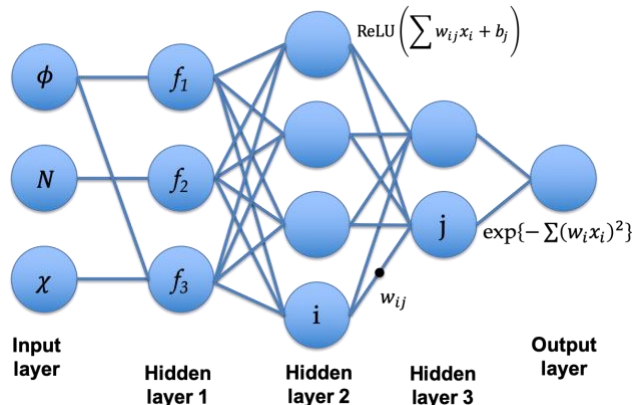


FIG. 1 Deep neural network for the phase behavior of polymer-containing liquid mixtures. Hidden layer 1 captures the significance of physical properties. This layer may also be fully connected with the input layer. Hidden layers 2 and 3 serve as standard layers.

Our DNN for both polymer solutions and diblock copolymer melts consists of three hidden layers (FIG. 1). In this study, we use three, ten, and two neurons in hidden layers 1, 2, and 3, respectively. For the input x in hidden layers 2 and 3, we use the rectified linear unit (ReLU) $\text{ReLU}(\sum w_{ij} x_i + b_j)$ for activation functions with weight w_{ij} and bias b_j . The key component in the DNN is hidden layer 1, which captures the significance of physical properties and thus “speculates” the characteristic features of the phase behaviors. Here, the Flory-Huggins theory for

polymer solutions suggests that (a) the overall trend of spinodal curves for phase instability is substantially affected by the difference in the translational entropy between polymers and solvents, (b) the chain length of polymers (or the degree of polymerization) plays a crucial role in producing asymmetry in the shapes of spinodal curves and thus in determining the location of the critical point, and (c) the phase boundary is determined by a delicate balance between the entropy and enthalpy of polymers and solvents. Accordingly, we cast these three pieces of information into nonlinear functions: $f_1 = \phi \ln(\phi) / [(1-\phi) \ln(1-\phi)]$, $f_2 = 1/N$, and $f_3 = \chi \phi(1-\phi)$, where ϕ , N , and χ designate the volume fraction of polymers, the chain length of polymers, and the Flory parameter for measuring immiscibility between species, respectively. f_1 and f_3 calculate the ratio of the translational entropies of incompressible polymers and solvents and the enthalpic contribution to the free energy, respectively. Given that M is the number of training data points, a loss function is defined as the relative error $\sum \sigma_i / M$. Here, $\sigma_i = 1$ if the estimated and true values are different; otherwise, $\sigma_i = 0$. We minimize the loss function by randomly searching the weights [21]. To examine the efficacy of hidden layer 1, we consider the following patterns: f_1 is replaced by $\phi \ln(\phi)$ (pattern 1) and $f_1 = \phi$, $f_2 = N$ and $f_3 = \chi$ (pattern 2). We terminate a random search if the relative error is larger than 8% when 2×10^6 trials are performed. The success rate of the intact form is estimated at 8.7% from more than 20000 samples, but that of pattern 1 and pattern 2 is 0%. Thus, pattern 1 and pattern 2 are unsuccessful because they do not account for information about the balance between the entropies of polymers and solvents.

Note that standard neurons with activation functions transmit a signal to other neurons when the strength of the signal exceeds a certain threshold. Thus, the mean-field theory and scaling laws incorporated in hidden layer 1 evaluate the qualities of the physical properties and transform them into signals for hidden layer 2. If the signals are significant enough to exceed the threshold in the activation functions, then they will be further transmitted to other neurons.

The output layer determines the phase behavior of polymer solutions by calculating a Gaussian function, $y = \exp\{-\sum(w_i x_i)^2\}$. Here, a disordered phase (DIS) is assigned when the output $y < 0.5$; otherwise, macroscopic phase separation is assigned. Note that we obtain macroscopic phase separation when all weights w_i are zero. Thus, gradually increasing the weights w_i from zero indicates that the DNN initially fits the training data points for macroscopic phase separation and then gradually tunes the weights for DIS. Indeed, this fact provides a computational advantage in performing a random search for the weights w_i . Thus, we generate the initial values of w_i from -1 to 1 and then perform random searches by calculating $w_i \rightarrow w_i \pm \Delta$, where Δ is a uniform random

number between -1 and 1. If relative errors are large after a certain number of trials, then we discard the trial process and generate another initial value. This approach is because training datasets often involve the deep local minima of the loss function. However, if the initial values are appropriately set, then a random search can be finished shortly; for example, in certain cases, the search can be finished even within a few seconds. Here, the current study employed standard CPU cores (Intel Sandy Bridge E5-2670 2.60 GHz or equivalent). Hidden layer 1 allows us to promptly reach relative errors of less than 5%. The computational time for a single run typically ranges from a few seconds to no more than a few hours throughout this article. Thus, our random search with the Gaussian function is computationally feasible on standard workstations.

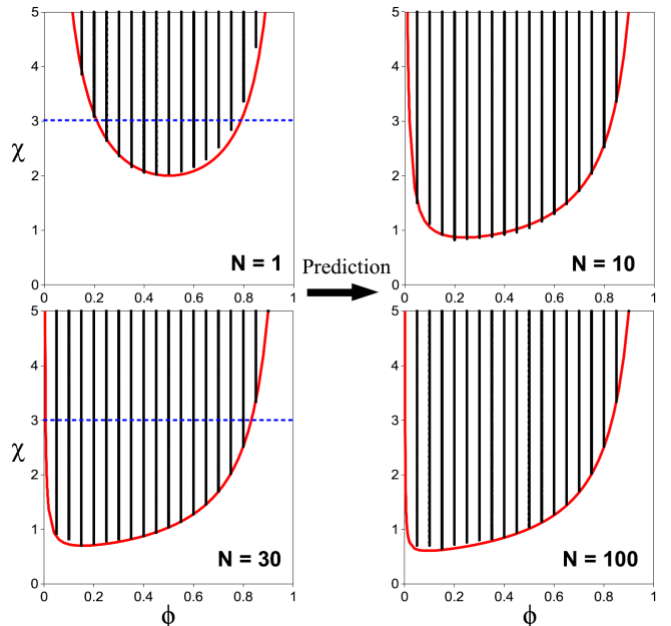


FIG. 2 Phase diagrams of polymer solutions. The training data points exist below $\chi = 3$ (blue dashed lines in the left two figures). The DNN generates the black regions for macroscopic phase separation, which consist of dense data points that form “strip” structures in the y-direction. The Flory-Huggins theory provides the spinodal curves (red solid lines), above which macroscopic phase separation occurs. The DNN predicts the right two figures.

We provide the training and test datasets for the phase behavior using the Flory-Huggins theory as follows: The intervals of ϕ and χ are 0.05, and ϕ and χ range from 0 to 1 and 0 to 3, respectively. The chain lengths are $N=1$ for nonpolymeric liquids and 30 for polymer solutions. Figure 2 shows the phase diagrams produced by the DNN. The relative error is 0.094%. The agreement between the predictions of the DNN and the test datasets is excellent within $\chi \leq 3$. The DNN also predicts the phase behaviors for $N = 1$ and 30 in the range of $3 < \chi \leq 5$, and the results are in excellent agreement with the test datasets. Moreover, the DNN predicts the phase behaviors for $N=10$ and 100 remarkably accurately.

We can also directly apply our DNN shown in FIG. 1 to the phase behavior of incompressible, symmetric diblock copolymer melts. The inputs are the volume fraction of block A ϕ , the chain lengths of blocks A and B N , and the Flory parameter χ . Thus, no essential changes in the DNN for polymer solutions are necessary. The value y of the Gaussian function in the output layer is defined as follows: $0 < y \leq 0.2$ for DIS, $0.2 < y \leq 0.4$ for body-centered-cubic phases (BCC), $0.4 < y \leq 0.6$ for hexagonally close-packed sphere phases (HCP), $0.6 < y \leq 0.8$ for gyroid phases (GYR), and $0.8 < y \leq 1$ for lamellar phases (LAM). We consider the following characteristic features of the phase behavior of diblock copolymer melts: (a) the translational entropy of each block, (b) the enthalpic interaction between the two blocks, and (c) the interfacial width between the two blocks in the ordered structures. A scaling law suggests that the interfacial width in the ordered structures scales with $\approx (N\chi)^{-0.5}$ for weakly segregated diblock copolymers [22]. Accordingly, we set $f_1 = \phi \ln(\phi) + (1 - \phi) \ln(1 - \phi)$, $f_2 = \chi\phi(1 - \phi)$, and $f_3 = (N\chi)^{-0.5}$. The optimization performance was not sensitive to the exponent in f_3 . This study also examined several other patterns for f_i , which did not adequately capture the qualitative features of block copolymer melts, but those patterns failed to tune the DNN. However, once the f_i suggested above was used, the performance drastically increased, and tuning the weights with high accuracy became achievable. To evaluate the efficacy of f_i , a random search was terminated after 5×10^7 trials if the relative error was larger than 5%. The success rate was 0.23% out of 3047 trials, whereas that of the other patterns was 0%.

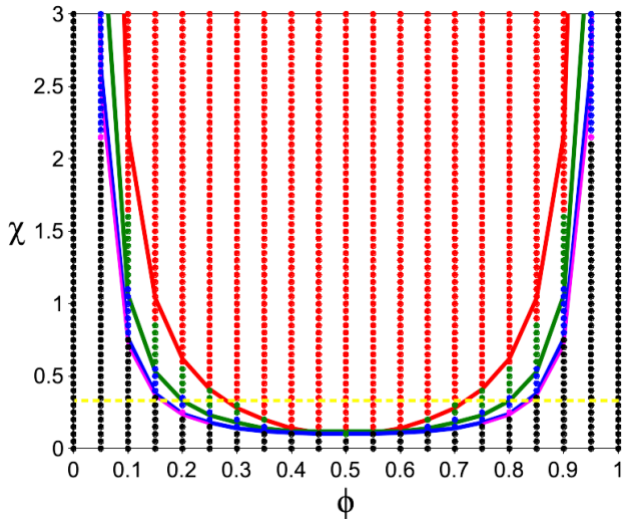


FIG. 3 Phase diagram of diblock copolymer melts. The training dataset exists below $\chi = 0.3$ (yellow dashed line). The DNN predicts the phase behavior above $\chi = 0.3$. The Landau theory provides the phase boundaries between GYR and LAM (red), HCP and GYR (green), BCC and HCP (blue), and DIS and BCC (purple). Data points: LAM (red), GYR (green), HCP (blue), BCC (purple), and DIS (black).

The training and test datasets for the phase behavior were produced using the Landau theory of microphase separation developed by Leibler [23] and Hamley and Podnec [24]. The training dataset consists of 365 data points in $0 \leq \phi \leq 1$ and $0 \leq \chi \leq 0.3$. The chain length of a block copolymer is $N=100$. Figure 3 shows the phase diagram drawn by the DNN. The relative error is 3.84%. The predictions of the DNN in $0.3 < \chi \leq 3$ are remarkably consistent with the test dataset. The test dataset shows that BCC exists between the purple and blue lines, but this area is quite narrow. Nevertheless, the DNN also adequately captures this feature and compares favorably with the test dataset, providing purple dots for BCC at, for example, $\phi = 0.05$ and 0.95 . This study examined several other sets of weights with relative errors less than 5%, and the predictive power was equivalently good when $\chi \leq 2$. Thus, the predictions of the DNN are relatively robust in considering the phase behavior of block copolymer melts.

We also examine the efficacy and predictive power of our DNN for experiments, taking the phase behavior of lithium salt-doped PEO-b-PS diblock copolymer melts as an example [25]. This system exhibits the disorder-order and various order-order phase transitions. However, reproducing the experimental observations and understanding the true nature of the phase behaviors by existing theories and molecular simulations remain significantly limited, primarily because both computational and theoretical modeling and calculations are challenging. Note that the microphase separation of this system can be characterized by (a) the translational entropy of the salt ions $r \ln r$, (b) the enthalpic contribution due to the solvation energy of the salt ions, and (c) the interfacial width between the two blocks $(N\chi_{\text{eff}})^{-0.5}$. Here, r is the salt loading defined as the ratio of the Li^+ and EO monomer concentrations $r = [\text{Li}^+]/[\text{EO}]$, and χ_{eff} is the effective Flory parameter for the salt-doped block copolymers and shown to scale as $(\chi_{\text{eff}} - \chi) \propto r$ experimentally [25,26] and theoretically [27]. Mean-field theory suggests that the Born solvation energy, which is proportional to the salt concentration r , qualitatively accounts for the experimental data [27]. Accordingly, we set $f_1 = r \ln r$, $f_2 = ar$ according to the Born solvation energy form, and $f_3 = (N\chi_{\text{eff}})^{-0.5}$, where $\chi_{\text{eff}} = \chi + br$. Both experimental and theoretical studies have suggested that b is on the order of unity; thus, we use $b = 1$. The Born solvation energy suggests that a is on the order of 10; thus, we use $a = 15$. Here, a varied from $a = 1$ to $a = 100$, but there was no substantial difference in optimization speed. As in the cases of the polymer solutions and the salt-free diblock copolymer melts, we also examined six arbitrary patterns for the f_i (TABLE I), which resulted in significantly poor success rates. Figure 4(a) illustrates our training dataset consisting of 567 data points constructed from Ref. [25]. The DNN used in FIG. 4(b) is tuned with a relative error of 5% and corresponds reasonably well with the experimental data. Although this study examined more than ten other sets

of weights with similar accuracy, most of the results compared favorably with the experimental data.

TABLE I. *Unsuccessful* trial patterns of the f_i vs. the success rate. A random search was terminated after 5×10^7 trials if the relative error was larger than 10%.

	f_1	f_2	f_3	Success rate %
Pattern 1	ϕ	N	χ	0
Pattern 2	ϕ/N	$1/N$	$\phi\chi$	0
Pattern 3	ϕ/N	0	$\phi\chi$	0
Pattern 4	ϕ	$1/N$	χ/ϕ	0
Pattern 5	ϕ	$1/N$	$\phi + \chi$	0
Pattern 6	$\ln \phi$	15ϕ	$1/\sqrt{N(\phi + \chi)}$	0.03

Of particular interest is the predictive power of the DNN when experimental data points are limited. To this end, we consider two limiting cases anticipated from statistical thermodynamics as follows: (1) The phase behavior exhibits DIS in the high-temperature limit, and (2) when the salt concentration is high enough to form an ionic liquid and no additional interaction is considered, the system becomes a dilute block copolymer solution and should exhibit DIS. In the current study, we add these data points to the training datasets as a regularization scheme [28].

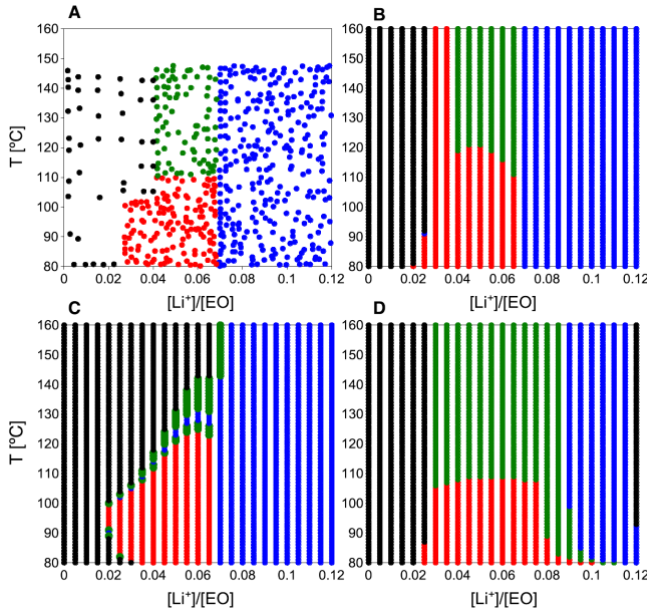


FIG. 4 Phase diagrams of lithium salt-doped PEO-b-PS melts. DIS (black), LAM (red), GYR (green), and HCP (blue). (A) The experimental results. (B) The DNN tuned with all the experimental data points. (C) The prediction of GYR. (D) The prediction of HCP. The relative errors are less than 5%. The DNN generates dense data points that form “strip” structures in the y-direction.

We first tune the DNN for only DIS, LAM, and HCP, not for GYR, with the additional data points from item (1). Figure 4(c) and (d) show our representative results. The DNN predicts GYR around the region at $[Li^+]/[EO] = 0.05$

and $T=130$ °C, as observed in the experiments. This study examined more than ten different types of weights with relative errors less than 5%, but all cases predicted GYR near this region. Here, the success rate became $2.028 \times (\%error) - 8.226$ when $(\%error) \lesssim 7.5\%$, whereas it significantly increases to 28% with $(\%error) = 8\%$. Similarly, using the additional data points from item (2), the DNN predicts that HCP occurs as the salt concentration increases. This result, including the overall trend of the phase boundary of HCP, also corresponds well with the experimental data shown in FIG. 4 (a). Here, nineteen out of twenty-three different sets of weights with relative errors less than 5% predicted HCP with reasonable salt concentrations and temperatures. We attribute these reasonable, robust predictions about GYR and HCP primarily to the addition of the data points from the limiting cases. For cross validation, we randomly obtained the training data points again, but the overall conclusion remains unchanged.

In conclusion, a hidden layer that captures thermodynamically important features via mean-field theory and scaling laws was incorporated into a DNN, thus allowing us to describe the phase behavior of polymer solutions and salt-free and salt-doped diblock copolymer melts. Appropriate construction of this layer significantly speeds up weight optimization and reduces the size of the DNNs, whereas the layer design is not unique. Given that the DNN is tuned, the phase diagrams can be reproduced without implementing advanced theories and molecular simulations. Moreover, our DNN has predictive power and can assist in exploring new phase behaviors in polymer-containing liquid mixtures.

Acknowledgments: We are grateful to the High-Performance Computing Shared Facility, Superior, at MTU for their essential support. This work was supported by the Research Excellence Fund of Michigan Technological University.

- [1] Y. LeCun, Y. Bengio, and G. Hinton, *Nature* **521**, 436 (2015).
- [2] M. S. Jorgensen, H. L. Mortensen, S. A. Meldgaard, E. L. Kolsbjerg, T. L. Jacobsen, K. H. Sorensen, and B. Hammer, *J. Chem. Phys.* **151** (2019).
- [3] S. Ibric, M. Jovanovic, Z. Djuric, J. Parojcic, L. Solomun, and B. Lucic, *J Pharm Pharmacol* **59**, 745 (2007).
- [4] T. Degim, J. Hadgraft, S. Ilbasimis, and Y. Ozkan, *J Pharm Sci* **92**, 656 (2003).
- [5] G. Pilania, C. C. Wang, X. Jiang, S. Rajasekaran, and R. Ramprasad, *Sci Rep-UK* **3** (2013).
- [6] B. S. Rem, N. Käming, M. Tarnowski, L. Asteria, Nick Fläschner, C. Becker, K. Sengstock, and C. Weitenberg, *Nat Phys* **15**, 917 (2019).
- [7] E. P. L. van Nieuwenburg, Y. H. Liu, and S. D. Huber, *Nat Phys* **13**, 435 (2017).
- [8] C. D. Li, D. R. Tan, and F. J. Jiang, *Ann Phys-New York* **391**, 312 (2018).
- [9] Q. S. Wei, R. G. Melko, and J. Z. Y. Chen, *Physical Review E* **95** (2017).
- [10] M. Gao, L. T. Yin, and J. C. Ning, *Atmos Environ* **184**, 129 (2018).
- [11] A. Esteva, B. Kuprel, R. A. Novoa, J. Ko, S. M. Swetter, H. M. Blau, and S. Thrun, *Nature* **542**, 115 (2017).

- [12] T. J. Brinker *et al.*, *J Med Internet Res* **20** (2018).
- [13] S. Dai, B. G. Sumpter, and D. W. Noid, *J Phase Equilib* **16**, 493 (1995).
- [14] C. J. Richardson, A. Mbanefo, R. Aboofazeli, M. J. Lawrence, and D. J. Barlow, *J Colloid Interf Sci* **187**, 296 (1997).
- [15] L. Djekic, S. Ibric, and M. Primorac, *International Journal of Pharmaceutics* **361**, 41 (2008).
- [16] S. Agatonovic-Kustrin and R. G. Alany, *Pharmaceut Res* **18**, 1049 (2001).
- [17] S. Agatonovic-Kustrin, B. D. Glass, M. H. Wisch, and R. G. Alany, *Pharmaceut Res* **20**, 1760 (2003).
- [18] R. G. Alany, S. Agatonovic-Kustrin, T. Rades, and I. G. Tucker, *J Pharmaceut Biomed* **19**, 443 (1999).
- [19] A. Mendyk and R. Jachowicz, *Expert Syst Appl* **32**, 1124 (2007).
- [20] S. Agatonovic-Kustrin, D. W. Morton, and R. Singh, *Colloid Surface A* **415**, 59 (2012).
- [21] J. Bergstra and Y. Bengio, *J Mach Learn Res* **13**, 281 (2012).
- [22] E. Helfand and Y. Tagami, *J. Chem. Phys.* **56**, 3592 (1972).
- [23] L. Leibler, *Macromolecules* **13**, 1602 (1980).
- [24] I. W. Hamley and V. E. Podnests, *Macromolecules* **30**, 3701 (1997).
- [25] N. S. Wanakule, J. M. Virgili, A. A. Teran, Z.-G. Wang, and N. P. Balsara, *Macromolecules* **43**, 8282 (2010).
- [26] W. S. Young, J. N. L. Albert, A. B. Schantz, and T. H. Epps, *Macromolecules* **44**, 8116 (2011).
- [27] I. Nakamura, N. P. Balsara, and Z.-G. Wang, *Phys. Rev. Lett.* **107**, 198301 (2011).
- [28] J. Schmidhuber, *Neural Networks* **61**, 85 (2015).